

Quantum Geometry of Altermagnetic Magnons Probed by Light

Rundong Yuan,^{1,*} Wojciech J. Jankowski,^{1,†} Ka Shen,^{2,3} and Robert-Jan Slager^{4,1,‡}

¹*TCM Group, Cavendish Laboratory, University of Cambridge,
J. J. Thomson Avenue, Cambridge CB3 0HE, United Kingdom*

²*The Center for Advanced Quantum Studies and School of Physics and Astronomy,
Beijing Normal University, Beijing 100875, China*

³*Key Laboratory of Multiscale Spin Physics, Ministry of Education,
Beijing Normal University, Beijing 100875, China*

⁴*Department of Physics and Astronomy, University of Manchester,
Oxford Road, Manchester M13 9PL, United Kingdom*

(Dated: August 6, 2025)

Magnons with momentum-dependent chirality are a key signature of altermagnets. We identify bicircular light as a smoking-gun optical probe for chiral altermagnetic magnons, selectively targeting their quantum geometry induced by an alteration of magnonic chirality. We show that in d -wave altermagnets, under a canting magnetic field, the altermagnetic magnons realize a nontrivial quantum geometry, resulting in an enhancement of the nonlinear second-order light-magnon interactions. We find that the scattering of bicircular pulses probes the present magnon quantum geometry, even if the magnonic topology is trivial. Hence, our findings establish bicircular Raman response as an optical effect of choice to identify altermagnetic magnons. As such, we propose a universal experimental protocol to distinguish altermagnets from antiferromagnets by detecting their magnon chirality patterns with light, independently of the underlying magnon topology.

Introduction.— Excitations in ordered media, such as magnets, provide insights into the physical character of the underlying order. Magnons, the quanta of spin waves, possess spin-precessional information in magnetic materials, as excitations of magnetic ground states [1–3]. Due to the time-reversal symmetry (TRS) breaking in ferromagnets, only right-handed (RH) magnons exist upon exciting a ferromagnetic ground state. As such, this results in chiral phenomena in ferromagnets, as determined by the direction of spontaneous magnetization [4–9]. The chirality of ferromagnetic magnons can be revealed by nonreciprocal magnon propagation [4–6], or by magnon spin current with only one sign under a fixed magnetic field [7–9]. On the other hand, the left-handed (LH) magnon chirality is recovered in antiferromagnetic (AFM) ground states, given their pseudo-TRS [10–13].

In a recently proposed class of magnetic materials [14–16], altermagnets (AMs), the excitations of their magnetic order, i.e., altermagnetic magnons, possess chiral properties despite a vanishing net magnetic moment of the system, even without any relativistic effects [14, 17–19]. Unlike AFMs, the AMs break TRS by their spin space groups, and thus lift both electronic and magnonic band structure degeneracies, according to their magnetic polarizations or chiralities [14, 17, 18, 20–23]. Specifically, in AMs, the RH and LH magnons are energetically lifted, without any external magnetic field along the Néel vector, nor with relativistic effects such as Dzyaloshinskii-Moriya interaction (DMI) [17, 24, 25], unlike their AFM counterparts [26]. This splitting of AM magnons can be accounted for by the asymmetric exchange interactions between magnetic atoms [14, 17–19]. The chirality of magnetic excitations distinguishes AMs

from AFMs, and thus gives insight into the classification of magnetic order on a lattice, which makes the detection of magnon chirality highly desirable [18, 27].

The chiral magnons in AMs have been investigated theoretically in various types of altermagnets such as d -wave altermagnet RuO_2 [17], Mn_2SeTe [28], etc., and g -wave altermagnets such as MnTe [19], CrSb [29], Fe_2O_3 [30]. A full classification of magnons can be dictated by the spin space group classifications [31–35], following similar strategies for (magnetic) space groups [36–41]. Experimentally, the energy splitting of magnons has been observed by inelastic neutron scattering in the g -wave altermagnet $\alpha\text{-MnTe}$ [28], while their chirality has not been inspected to date. Notably, the split of magnon bands was found to be absent in altermagnetic MnF_2 [27]. Electrical detection of magnon chirality has been conducted in a g -wave altermagnet $\alpha\text{-Fe}_2\text{O}_3$ [42], but the excitation energy (~ 10 GHz) is much lower than the splitting of chiral magnon bands, thus, making their observations unlikely to originate from altermagnetism. To our best knowledge, a direct probe of the split chirality of AM magnons remains elusive until now. It should be stressed that the energy scale of chiral magnons is much higher than the range of electrical probes [42–45], whereas inelastic neutron scattering experiments are generally not sensitive to antiferromagnetic, or altermagnetic, magnon chirality [28, 46–48].

Centrally to this work, quantum geometry, consisting of the quantum metric and Berry curvature, can characterize the momentum-space Riemannian structure of Bloch wavefunctions arising from a given Hamiltonian [49, 50]. Nontrivial geometry is found to give rise to Hall conductances [51–55], nonlinear transport [56, 57], and higher-order optical responses [55, 58–62] in vari-

ous materials. In AMs, electronic quantum geometry has been reported to induce nontrivial topology [63, 64], nonlinear electron transport [65, 66], and Raman dichroism signatures [67]. On another note, bicircular light (BCL), which targets information of different symmetry by its phase slip and frequency tunability, has been utilized to probe quantum geometries [68–70]. For magnons, the nontrivial topology of AFM spin waves could also be captured by light-matter interactions with a canting (perpendicular) magnetic field and relativistic effects [61]. Although yet to be explored, light-matter interaction underpinned by the magnonic quantum metric, rather than the Berry curvature [61, 71–75], promises to be pivotal for capturing geometrical properties of magnons. Whether a universal relation exists between magnon chirality distribution in AMs and magnonic quantum geometry is an open question, which we address here with a positive and general answer.

As shown in Fig. 1(a), we establish an optical probe of chiral altermagnetic magnons and their quantum geometry with bicircular light ($\gamma_R + \gamma_L$) in an altermagnet canted by a magnetic field. We validate our findings in systems with trivial magnonic topology, i.e., realizing trivial magnonic Chern numbers [61], in a minimal d -wave altermagnetic Heisenberg model. After applying a canting magnetic field, a splitting of magnonic nodal line is found to appear at Γ -M high-symmetry line where the LH and RH magnons hybridize. We show that in the first Brillouin zone (BZ), the magnon chirality switches as a function of the wavevector \mathbf{k} . As a consequence, the alternating chirality of AM magnons in the Bloch space gives rise to the nontrivial geometry of magnon bands, alongside the presence of trivial band topology, which we reveal with accumulated phases in magnonic Wilson loop. We deduce an enhancement of light-matter coupling through quantum metric in the dominant second and subleading fourth order terms. Within our approach, the quantum geometry of AM magnons is revealed as accessible to be probed by nonlinear bicircular Raman spectroscopy. Such effects are found to be unique to the altermagnetic systems, and are absent in the antiferromagnetic ones, as we further demonstrate.

Modelling altermagnetic magnons.— We start from a minimal d -wave altermagnetic spin-lattice tight-binding model to investigate the altermagnetic magnons [76]. We consider an altermagnetic Heisenberg model canted by an external magnetic field without DMI, see End Matter for technical details. The model includes magnetic crystalline anisotropy to stabilize the magnetizations. As shown in the left panel of Fig. 1(a), the considered spin Hamiltonian preserves a $C_{4z}T||C_2$ symmetry without an external magnetic field, as expected for a d -wave altermagnetic spin model. Setting altermagnetic splitting $\Delta J = 0$, we can restore pseudo-TRS in the model and yield an AFM ground state. In the following, we will also

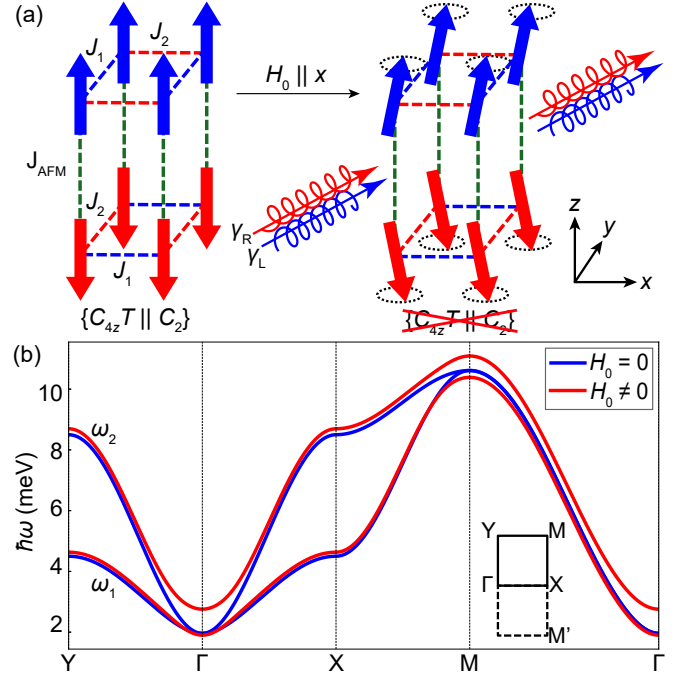


FIG. 1. Modelling altermagnetic magnons with split chirality. (a) Minimal spin model for d -wave altermagnetic magnons, canted by an external magnetic field. The spin structures before (left) and after (right) applying a canting field are presented. The altermagnetic magnons are bicircularly probed by photons of opposite handedness ($\gamma_{L/R}$). (b) Magnonic band structure with external canting field (red lines) and without (blue lines). Here, we set: $S = 1$, with couplings $J = 1$ meV, $\Delta J = 0.5$ meV, $J_{\text{AFM}} = 2.0$ meV, $K = 0.8$ meV, as detailed in the End Matter. We choose $H_0 \neq 0$ to match the energy scale of 2 meV.

show that the nontrivial geometrical effects are present regardless of the scale of exchange interactions, but only rely on the altermagnetic symmetry.

We use a Holstein-Primakoff (HP) transformation for our altermagnetic model [61, 71, 77]: $S_{x,i}^\dagger + iS_{y,i}^\dagger = \sqrt{2S}a_i$, $S_{x,i}^\dagger - iS_{y,i}^\dagger = \sqrt{2S}a_i^\dagger$, $S_{x,i}^\dagger + iS_{y,i}^\dagger = \sqrt{2S}b_i$, and $S_{x,i}^\dagger - iS_{y,i}^\dagger = \sqrt{2S}b_i^\dagger$, where a_i, b_i (a_i^\dagger, b_i^\dagger) are magnon annihilation (creation) operators at the lattice sites i . Transforming the basis into Bloch space as $a_i = 1/\sqrt{N} \sum_{\mathbf{k}} a_{\mathbf{k}} e^{-i\mathbf{k} \cdot \mathbf{r}_i}$ with position vectors \mathbf{r}_i , and analogously for the b_i , we obtain the quadratic bosonic Hamiltonian in the basis $\psi_{\mathbf{k}} = (a_{\mathbf{k}}, b_{\mathbf{k}}, a_{-\mathbf{k}}^\dagger, b_{-\mathbf{k}}^\dagger)^T$, with a linear-wave approximation. We only consider the in-plane wavevector $\mathbf{k} = (k_x, k_y)$ of magnons. The eigenmodes are obtained by a bosonic Bogoliubov de-Gennes (BdG) transformation, $\psi_{\mathbf{k}} = U\phi_{\mathbf{k}}$, in which $\phi_{\mathbf{k}} = (\alpha_{\mathbf{k}}, \beta_{\mathbf{k}}, \alpha_{-\mathbf{k}}^\dagger, \beta_{-\mathbf{k}}^\dagger)^T$ denotes the eigenmode basis. U is a paraunitary matrix normalized by $U^\dagger \bar{U} = I$, where $\bar{U} = \tau_3 U \tau_3$. Utilizing the Cholesky decomposition approach of bosonic

operators, we obtain the connection matrix U that diagonalizes the Hamiltonian $\mathcal{H}^{\mathbf{k}}$, $U^\dagger \mathcal{H}^{\mathbf{k}} U = \Omega^{\mathbf{k}}$ [78] (see End Matter), and the magnonic eigenenergy matrix, $\Omega^{\mathbf{k}} = \text{diag}(\omega_1(\mathbf{k}), \omega_2(\mathbf{k}), \omega_1(-\mathbf{k}), \omega_2(-\mathbf{k}))$. Here, $\omega_i(\mathbf{k})$, with $i = 1, 2$, denote the energies of magnons with a wavevector \mathbf{k} . The model supports $\omega_i(\mathbf{k}) = \omega_i(-\mathbf{k})$, as it obeys the C_{2z} symmetry. This culminates in $(C_{4z}T)^2 = 1$, which indicates a trivial topology of considered magnon bands, since the symmetry obstructs the existence of nontrivial Pfaffian operators at high-symmetry points [79]. Moreover, our model can be adiabatically transformed into a nonrelativistic antiferromagnetic model, while preserving the $C_{4z}T$ symmetry, meaning that both belong to the same topological class. It has been experimentally investigated that the nonrelativistic antiferromagnetic magnons have trivial topology [15, 80, 81], consistently with the model studied hereby, which realizes topologically-trivial magnons.

In Fig. 1(b), we show the magnonic band structure of the d -wave AM model with and without the perpendicular magnetic field (red/blue lines). The high-symmetry points are defined in the right-lower panel of Fig. 1(b). Consistently with previous findings [17, 28, 76], we find split chirality for magnonic bands. Without an external magnetic field, a magnonic nodal line appears at the Γ -M high-symmetry line, and a Dirac-type band touching appears at the Γ point. The perpendicular field lifts the degeneracy at the nodal line and at the Γ point, which aligns with our expectation, since the field breaks the $C_{4z}T||C_2$ symmetry, as shown in Fig. 1(a)–Fig. 1(b).

Chirality and quantum geometry of altermagnetic magnons.— Since the split altermagnetic magnon bands are chiral [17], it is important to quantify their chirality p_j , which is shown in Fig. 2(a)–Fig. 2(b). The magnonic chirality can be calculated by the difference between the amplitude of RH and LH magnons, with $p_j \equiv \sum_{i,\text{RH}} |U_{ij}^{-1}|^2 - \sum_{i,\text{LH}} |U_{ij}^{-1}|^2$ [17]. Owing to the normalization of the connection matrix, here $p_j = \pm 1$ represents a fully RH (LH) magnon chirality, and $p_j = 0$ represents a linear polarization. On the high-symmetry line Γ -M, one can observe that although the magnonic bands are lifted, the chirality of both bands is similarly linear in our model. What is more, the distribution of chirality p_j over the first BZ behaves distinctly in AM and AFM, see Supplemental Material (SM) for details [82].

We emphasize that the LH and RH characters of magnons are directly captured by the amplitudes in the original basis ($a_{\mathbf{k}}/b_{\mathbf{k}}$) of the system, i.e., in the column of the BdG matrix which denotes the eigenvectors of magnons in the Bloch space. Meanwhile, given the alternating feature of p_j in momentum space, it is worth inspecting quantum-geometric consequences of the distribution of magnon chirality, since the quantum geometry relies on the differential features of the eigenvectors [49, 50]. To formally characterize the geometry and

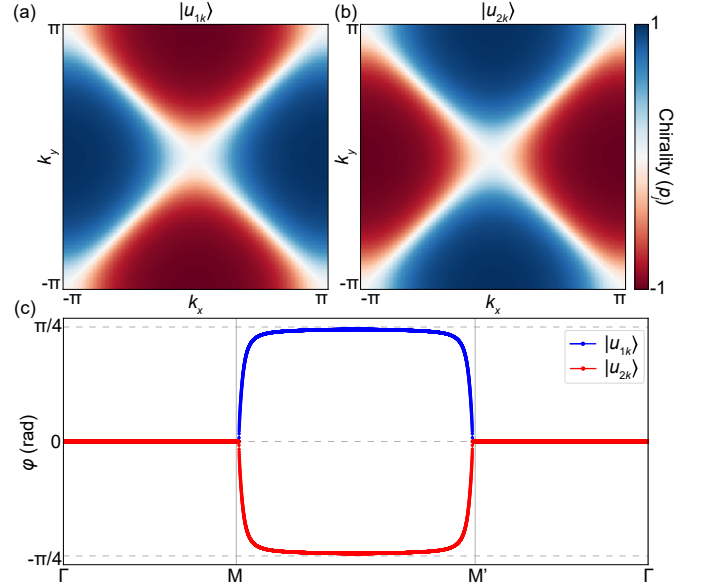


FIG. 2. Interplay of magnonic chirality and quantum geometry in altermagnets. (a)–(b) The chirality of lower and upper magnonic bands $|u_{1\mathbf{k}}\rangle \equiv [U(\mathbf{k})]_1$, $|u_{2\mathbf{k}}\rangle \equiv [U(\mathbf{k})]_2$. The magnon chirality over momentum space (p_j) is presented, with the blue and red colors representing the RH and LH chirality, respectively. (c) Magnonic Wilson lines along IBZ. The blue and red curves denote Wilson lines for $|u_{1\mathbf{k}}\rangle$ and $|u_{2\mathbf{k}}\rangle$. In the above, we use the same parameters as in Fig. 1 in the presence of external magnetic field ($H_0 \neq 0$).

topology of the modeled altermagnetic magnons, we first calculate the magnonic Wilson loop surrounding the irreducible Brillouin zone (IBZ) [79], as shown in Fig. 2(c). The Wilson loop is calculated from the phases of the Wilson line: $W(\mathbf{k}) = \prod_{\partial\text{IBZ}} \bar{U}^\dagger(\mathbf{k}_{i+1}) U(\mathbf{k}_i)$, where \mathbf{k}_i denote the wavevectors at different points of the Wilson loop contour. Importantly, we use a different definition from fermionic Wilson loop, since the overlap of neighbor bosonic eigenvector should be represented by $\bar{U}(\mathbf{k}_1) U(\mathbf{k}_2)$. The magnonic Wilson loop eigenvalue moves from $\phi = 0$ to $\phi = \pm\pi/4$, and back to $\phi = 0$, which indicates the eigenvectors of the magnon bands accumulate a Berry phase which is subsequently dissolved around the loop over the boundary of IBZ, see Fig. 2(c). The magnonic Wilson loops are not winding around the IBZ, in agreement with our previous discussion of topology. Meanwhile, in an antiferromagnetic model, the Wilson loop does not possess any nontrivial accumulated phases (see SM [82]), consistently with a trivial quantum geometry, see End Matter. The geometrical difference pinpointed by the Wilson loop can be attributed to the unconventional chiral nature of the altermagnetic magnons, i.e., the chirality alteration in the IBZ amounts to an alternating pattern of magnonic eigenvector orientation [Fig. 2(a)–Fig. 2(b)], which realizes nontrivial geometry.

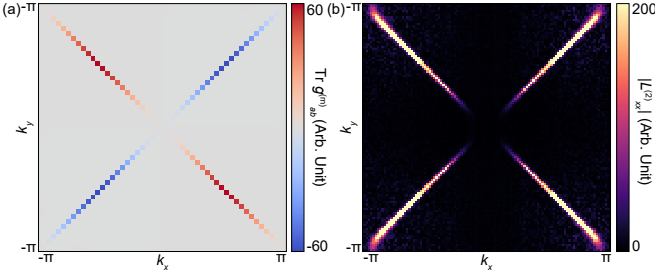


FIG. 3. **Quantum metric and nonlinear light-magnon coupling in a d -wave altermagnet.** (a) The quantum metric of magnons $g_{ab}^{(m)}$ in the lower band of a minimal d -wave spin Hamiltonian canted by an external magnetic field, over the first Brillouin zone. The trace of the magnonic metric $[\text{Tr } g_{ab}^{(m)}]$ peaks at the chirality (p_j) crossover boundary. (b) The momentum-space features of the second-order light-magnon coupling $L_{ab}^{(2)}$. We find that $L_{ab}^{(2)}$, which is governed by the magnonic quantum metric, is enhanced at the magnon chirality crossover regions.

We further confirm that the topologically-trivial altermagnetic magnons carry nontrivial quantum geometry, by an explicit evaluation of the quantum metric tensor, see Fig. 3(a). Formally, the quantum geometry of magnons is captured by magnonic quantum geometric tensor (mQGT), $Q_{ij}^{(m)} = g_{ij}^{(m)} - \frac{i}{2} \Omega_{ij}^{(m)}$ [61]. In particular, the magnonic Berry curvature $\Omega_{ij}^{(m)}$, which naturally presents in topologically nontrivial magnons such as Chern magnons, can be characterized by dichroic Raman scattering [61]. Nevertheless, for topologically-trivial magnons, as considered in our work, the presence of any Berry curvature is not underpinned by Chern topology. Here, the only characteristic signature arising from the unique alteration of chirality of altermagnons across BZ [17] is the nontrivial magnonic quantum metric $g_{ab}^{(m)}$, see End Matter. Given that the quantum metric $g_{ab}^{(m)}$ can also be probed by light-matter coupling [61], analogously to the electronic quantum metric [57, 62], we focus on the magnonic metric-induced optical features associated with the nonlinear light-magnon coupling in the following.

Nonlinear light-magnon coupling in altermagnets.— We now construct a methodology to probe the retrieved quantum geometry in altermagnetic magnons with light. Any light-matter interactions that are sensitive to the local quantum geometry of Hamiltonian over \mathbf{k} -space could be a promising candidate. We consider the light-matter coupling (LMC) Hamiltonian [59, 61] up to the fourth-order terms (see SM) [82], $\mathcal{H}^{\mathbf{k}}(\mathbf{A}) = \mathcal{H}^{\mathbf{k}} + L_a^{(1)} A_a + L_{ab}^{(2)} A_a A_b + \dots$, where $\mathbf{A} = (A_x, A_y)$ is the gauge potential vector, and a, b represent the directions x, y . Using perturbation theory in the LMC for magnons [83], we retrieve the first-

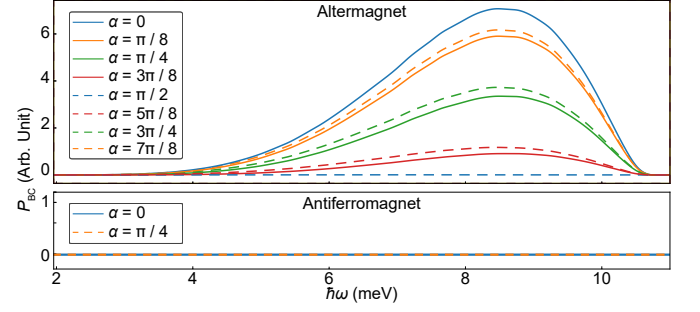


FIG. 4. **Probing light-magnon coupling with bicircular light.** We consider bicircular light of frequency ω_{in} with phase shift α between left- and right- circular components, inelastically scattered to frequency ω_{sc} , on experiencing a Raman shift $\omega = \omega_{\text{in}} - \omega_{\text{sc}}$. Resolution of the light-altermagnetic magnon cross-section P_{BC} capturing the scattering of altermagnetic magnons from light against α and ω allows to retrieve $L_{ab}^{(2)}$ enhanced by the magnon quantum metric $g_{ab}^{(m)}$ reflecting the altermagnetic magnon chirality pattern.

order and second-order terms $L_a^{(1)}, L_{ab}^{(2)}$ that read [61, 82],

$$\begin{aligned} L_a^{(1)} &= -\Omega_a - U^\dagger \bar{U}_a \Omega + \Omega \bar{U}^\dagger U_a, \\ L_{ab}^{(2)} &= L_a^{(1)} \bar{U}^\dagger U_b - \frac{1}{2} \Omega \bar{U}^\dagger U_{ab} \\ &\quad + \frac{1}{2} U^\dagger \bar{U}_{ab} \Omega + U^\dagger \bar{U}_a \Omega_b + \frac{1}{2} \Omega_{ab} + (a, b \rightarrow b, a), \end{aligned} \quad (1)$$

where the footnotes a, b introduced in the right-hand side gives $U_a \equiv \partial_{k_a} U$, $U_{ab} \equiv \partial_{k_a} \partial_{k_b} U$, and analogously for Ω_a, Ω_{ab} . Although the further contributions are negligibly small, they are also calculated up to the fourth order in terms of U_a for completeness, see SM [82]. One finds that the quantum metric enters in the first term of $L_{ab}^{(2)}$ [61], thus confirming that the emergent quantum metric in the magnon bands can enhance the nonlinear LMC [61], which we identify as a smoking-gun feature of an altermagnet. In Fig. 3, we show the distribution of quantum metric and LMC strength as a function of wavevector around the first BZ. In Fig. 3(a), the quantum metric is found to be maximal at the lifted Γ -M line. The absolute value of LMCs in the perturbative Hamiltonian is also calculated, and shown in Fig. 3(b). As expected, the LMC is enhanced around the metric maxima regions. Given the special geometry of studied light-magnon coupling, we now focus on the scattering experiments that are optically sensitive to the geometry of considered systems. Centrally to this work, we find that the BCL scattering is among the main candidates, given its tunability in terms of controllable phase relation α between two individual photon sources, which allows to target $L_{ab}^{(2)}$.

Probing altermagnetic magnons with bicircular light.— We now show how BCL can be used to probe the nontrivial magnonic geometry of altermagnetic magnons within realistic experimental setups. The BCL field takes

the form $\mathbf{A}(t) = \mathbf{A}_L e^{i(\eta\omega_{\text{in}}t + \alpha)} + \mathbf{A}_R e^{-i\omega_{\text{in}}t}$ [68, 69], with $\mathbf{E}_{L/R} = -\dot{\mathbf{A}}_{L/R}$, the electric field strengths of left/right-circularly-polarized light components with frequencies ω_{in} ($\eta = 1$). For $\alpha = 0$, the nonlinear LMC of altermagnetic magnons to linearly-polarized light is retrieved from the bicircular coupling. The combinations of left/right-circularly-polarized beams, yielding linearly-polarized light, have been previously proven successful in probing nontrivial electronic quantum geometry [84].

The BCL response is calculated in terms of the Raman scattering ($\omega_{\text{in}} \rightarrow \omega_{\text{sc}}$) cross-section $P_{\text{BC}} \propto |\bar{U} H_R U|^2 \delta(\omega_i - \omega_{\text{sc}} + \omega_{\text{in}})$ [61], where ω_i are the magnonic excitation energies, and H_R is the Raman scattering Hamiltonian given by $\mathcal{H}^{\mathbf{k}}(\mathbf{A})$, following the construction of Ref. [61]. To propose a credible realization for experiments, we assume that the incident and scattered photons have the same polarizations. We can reconstruct $L_{ab}^{(2)}$ on filtering out the first-order contribution $L_a^{(1)}$, which is distinctly sensitive to phase delay α of BCL (see SM [82]). In Fig. 4, we show how the light-magnon scattering cross-section P_{BC} [61] measured as a function of α allows to probe the magnon metric $g_{ab}^{(m)}$, which captures the momentum-space chirality crossovers unique to the altermagnetic magnons. Notably, we observe that the antiferromagnetic phase lacks similar features, see Fig. 4, consistently with their degenerate LH and RH chirality (see SM [82]).

Discussion and conclusions.— We now discuss the applicability of our results. Experimentally, the LMC effects of altermagnetic magnons could be realized in various types of d -wave altermagnetic materials, such as RuO_2 , given that our proposed experimental signatures do not rely on a specific type of lattice. It should be noted that other types of altermagnetic spin lattices, such as in honeycomb and checkboard altermagnets [63, 75], could accumulate nontrivial magnonic Berry phases and realize topological magnons. Nevertheless, we expect that such cases consistently result in nontrivial quantum geometry observable with BCL. Depending on the symmetry of the altermagnet, we expect enhancements with different symmetries over \mathbf{k} -space to be manifested in the scattering of BCL. Independently of the symmetry, our results clearly show that the LMC effects can distinguish AMs from AFMs due to a qualitative difference between the AM and AFM magnons.

In summary, we investigate magnonic quantum-geometry-induced optical effects to deduce the characteristic of an altermagnetic state, which we recognize as observable with bicircular light. We explicitly demonstrate our findings in a d -wave altermagnet model with a canting magnetic field. The canting magnetic field gives rise to a band gap at the magnonic nodal line (Γ -M line), along which the magnon quantum metric is enhanced, and which drives the nonlinear light-magnon coupling. We numerically confirm the nontrivial geometry to in-

duce LMC effects around the lifted nodal line. To understand an interplay of geometry and topology, we employ a Wilson loop calculation, which is consistent with the observations of trivial topology, but nontrivial geometry, in altermagnets. In the AFM ground states, the investigated optical effects are found to be absent. This observation puts the conventional antiferromagnets in contrast with altermagnets, in the light of our optically-selective proposal. Our findings provide a smoking-gun optical criterion for confirming the presence of altermagnetic order with unique spin excitations.

Acknowledgements.— We thank Bo Peng, Habib Rostami, Haiming Yu, and Yuelin Zhang for fruitful discussions. R.Y. acknowledges the support by CSC Scholarship No. 202408060249 and Cambridge Commonwealth, European, and International Trust. W.J.J. acknowledges funding from the Rod Smallwood Studentship at Trinity College, Cambridge. K.S. acknowledges National Natural Science Foundation of China (Grant No. 12374100) and the Fundamental Research Funds for the Central Universities. R.-J.S. acknowledges funding from an EP-SRC ERC underwrite grant EP/X025829/1 and a Royal Society exchange grant IES/R1/221060 as well as Trinity College, Cambridge.

* ry306@cam.ac.uk

† wjj25@cam.ac.uk

‡ rjs269@cam.ac.uk

- [1] V. V. Kruglyak, S. O. Demokritov, and D. Grundler, Magnonics, *J. Phys. D: Appl. Phys.* **43**, 264001 (2010).
- [2] A. V. Chumak, V. I. Vasyuchka, A. A. Serga, and B. Hillebrands, Magnon spintronics, *Nat. Phys.* **11**, 453 (2015).
- [3] A. Barman, G. Gubbiotti, S. Ladak, A. O. Adeyeye, M. Krawczyk, J. Gräfe, C. Adelman, S. Cotozana, A. Naeemi, V. I. Vasyuchka, *et al.*, The 2021 magnonics roadmap, *J. Phys.: Condens. Matter* **33**, 413001 (2021).
- [4] R. Damon and J. Eshbach, Magnetostatic modes of a ferromagnet slab, *J. Phys. Chem. Solids* **19**, 308 (1961).
- [5] J. Chen, T. Yu, C. Liu, T. Liu, M. Madami, K. Shen, J. Zhang, S. Tu, M. S. Alam, K. Xia, M. Wu, G. Gubbiotti, Y. M. Blanter, G. E. W. Bauer, and H. Yu, Excitation of unidirectional exchange spin waves by a nanoscale magnetic grating, *Phys. Rev. B* **100**, 104427 (2019).
- [6] T. Yu, Y. M. Blanter, and G. E. W. Bauer, Chiral pumping of spin waves, *Phys. Rev. Lett.* **123**, 247202 (2019).
- [7] K. Ando, S. Takahashi, J. Ieda, Y. Kajiwara, H. Nakayama, T. Yoshino, K. Harii, Y. Fujikawa, M. Matsuo, S. Maekawa, and E. Saitoh, Inverse spin-Hall effect induced by spin pumping in metallic system, *J. Appl. Phys.* **109**, 103913 (2011).
- [8] S. Maekawa, S. O. Valenzuela, E. Saitoh, and T. Kimura, *Spin Current* (Oxford University Press, 2017).
- [9] J. Wang, H. Wang, J. Chen, W. Legrand, P. Chen, L. Sheng, J. Xia, G. Lan, Y. Zhang, R. Yuan, J. Dong, X. Han, J. Ansermet, and H. Yu, Broad-wave-vector spin

- pumping of flat-band magnons, *Phys. Rev. Appl.* **21**, 044024 (2024).
- [10] R. Cheng, J. Xiao, Q. Niu, and A. Brataas, Spin pumping and spin-transfer torques in antiferromagnets, *Phys. Rev. Lett.* **113**, 057601 (2014).
 - [11] J. Li, C. B. Wilson, R. Cheng, M. Lohmann, M. Kavand, W. Yuan, M. Aldosary, N. Agladze, P. Wei, M. Sherwin, and J. Shi, Spin current from sub-terahertz-generated antiferromagnetic magnons, *Nature* **578**, 70 (2020).
 - [12] T. Wimmer, A. Kamra, J. Gückelhorn, M. Opel, S. Geprägs, R. Gross, H. Huebl, and M. Althammer, Observation of antiferromagnetic magnon pseudospin dynamics and the Hanle effect, *Phys. Rev. Lett.* **125**, 247204 (2020).
 - [13] P. Vaidya, S. A. Morley, J. van Tol, Y. Liu, R. Cheng, A. Brataas, D. Lederman, and E. del Barco, Subterahertz spin pumping from an insulating antiferromagnet, *Science* **368**, 160 (2020).
 - [14] L. Šmejkal, J. Sinova, and T. Jungwirth, Emerging research landscape of altermagnetism, *Physical Review X* **12**, 040501 (2022).
 - [15] L. Šmejkal, J. Sinova, and T. Jungwirth, Beyond conventional ferromagnetism and antiferromagnetism: A phase with nonrelativistic spin and crystal rotation symmetry, *Phys. Rev. X* **12**, 031042 (2022).
 - [16] C. Song, H. Bai, Z. Zhou, L. Han, H. Reichlova, J. H. Dil, J. Liu, X. Chen, and F. Pan, Altermagnets as a new class of functional materials, *Nat. Rev. Mater.* **10**, 473 (2025).
 - [17] L. Šmejkal, A. Marmodoro, K. Ahn, R. González-Hernández, I. Turek, S. Mankovsky, H. Ebert, S. W. D'Souza, O. Šipr, J. Sinova, and T. Jungwirth, Chiral magnons in altermagnetic RuO₂, *Phys. Rev. Lett.* **131**, 256703 (2023).
 - [18] Z. Liu, M. Ozeki, S. Asai, S. Itoh, and T. Masuda, Chiral split magnon in altermagnetic MnTe, *Phys. Rev. Lett.* **133**, 156702 (2024).
 - [19] L. M. Sandratskii, K. Carva, and V. M. Silkin, Direct *ab-initio* calculation of magnons in altermagnets: Method, spin-space symmetry aspects, and application to MnTe, *Phys. Rev. B* **111**, 184436 (2025).
 - [20] S. Reimers, L. Odenbreit, L. Šmejkal, V. N. Strocov, P. Constantinou, A. B. Hellenes, R. Jaeschke Ubiorgo, W. H. Campos, V. K. Bharadwaj, A. Chakraborty, M. Jourdan, *et al.*, Direct observation of altermagnetic band splitting in CrSb thin films, *Nat. Commun.* **15**, 2116 (2024).
 - [21] J. Ding, Z. Jiang, X. Chen, Z. Tao, Z. Liu, T. Li, J. Liu, J. Sun, J. Cheng, J. Liu, *et al.*, Large band splitting in g-wave altermagnet CrSb, *Phys. Rev. Lett.* **133**, 206401 (2024).
 - [22] J. Krempaský, L. Šmejkal, S. W. D'Souza, M. Hajlaoui, G. Springholz, K. Uhlířová, F. Alarab, P. C. Constantinou, V. N. Strocov, D. Usanov, *et al.*, Altermagnetic lifting of Kramers spin degeneracy, *Nature* **626**, 517 (2024).
 - [23] O. Fedchenko, J. Minár, A. Akashdeep, S. W. D'Souza, D. Vasilyev, O. Tkach, L. Odenbreit, Q. Nguyen, D. Kutnyakhov, N. Wind, *et al.*, Observation of time-reversal symmetry breaking in the band structure of altermagnetic RuO₂, *Sci. Adv.* **10**, eadj4883 (2024).
 - [24] A. Mook, J. Henk, and I. Mertig, Edge states in topological magnon insulators, *Phys. Rev. B* **90**, 024412 (2014).
 - [25] A. Mook, J. Henk, and I. Mertig, Magnon Hall effect and topology in kagome lattices: A theoretical investigation, *Phys. Rev. B* **89**, 134409 (2014).
 - [26] R. Cheng, M. W. Daniels, J.-G. Zhu, and D. Xiao, Antiferromagnetic spin wave field-effect transistor, *Sci. Rep.* **6**, 24223 (2016).
 - [27] V. C. Morano, Z. Maesen, S. E. Nikitin, J. Lass, D. G. Mazzone, and O. Zaharko, Absence of altermagnetic magnon band splitting in MnF₂, *Phys. Rev. Lett.* **134**, 226702 (2025).
 - [28] H. Yu, W. Feng, F. Zheng, and Y. Yao, Chiral magnons in an altermagnetic Janus Mn₂SeTe monolayer, *Comput. Mater. Today* **4**, 100021 (2024).
 - [29] Y. Zhang, X. Ni, K. Chen, and K. Cao, Chiral magnon splitting in altermagnetic CrSb from first principles, *Phys. Rev. B* **111**, 174451 (2025).
 - [30] R. Hoyer, P. P. Stavropoulos, A. Razpopov, R. Valentí, L. Šmejkal, and A. Mook, Altermagnetic splitting of magnons in hematite (α -Fe₂O₃), *arXiv preprint arXiv:2503.11623* (2025).
 - [31] X. Chen, Y. Liu, P. Liu, Y. Yu, J. Ren, J. Li, A. Zhang, and Q. Liu, Unconventional magnons in collinear magnets dictated by spin space groups, *Nature* **640**, 349 (2025).
 - [32] Y. Jiang, Z. Song, T. Zhu, Z. Fang, H. Weng, Z.-X. Liu, J. Yang, and C. Fang, Enumeration of spin-space groups: Toward a complete description of symmetries of magnetic orders, *Phys. Rev. X* **14**, 031039 (2024).
 - [33] Z. Xiao, J. Zhao, Y. Li, R. Shindou, and Z.-D. Song, Spin space groups: Full classification and applications, *Phys. Rev. X* **14**, 031037 (2024).
 - [34] X. Chen, J. Ren, Y. Zhu, Y. Yu, A. Zhang, P. Liu, J. Li, Y. Liu, C. Li, and Q. Liu, Enumeration and representation theory of spin space groups, *Phys. Rev. X* **14**, 031038 (2024).
 - [35] H. Schiff, A. Corticelli, A. Guerreiro, J. Romhányi, and P. A. McClarty, The crystallographic spin point groups and their representations, *SciPost Phys.* **18**, 109 (2025).
 - [36] J. Kruthoff, J. de Boer, J. van Wezel, C. L. Kane, and R.-J. Slager, Topological classification of crystalline insulators through band structure combinatorics, *Phys. Rev. X* **7**, 041069 (2017).
 - [37] H. C. Po, A. Vishwanath, and H. Watanabe, Symmetry-based indicators of band topology in the 230 space groups, *Nat. Commun.* **8**, 50 (2017).
 - [38] B. Bradlyn, L. Elcoro, J. Cano, M. G. Vergniory, Z. Wang, C. Felser, M. I. Aroyo, and B. A. Bernevig, Topological quantum chemistry, *Nature* **547**, 298 (2017).
 - [39] A. Bouhon, G. F. Lange, and R.-J. Slager, Topological correspondence between magnetic space group representations and subdimensions, *Phys. Rev. B* **103**, 245127 (2021).
 - [40] H. Watanabe, H. C. Po, and A. Vishwanath, Structure and topology of band structures in the 1651 magnetic space groups, *Science Advances* **4**, eaat8685 (2018).
 - [41] L. Elcoro, B. J. Wieder, Z. Song, Y. Xu, B. Bradlyn, and B. A. Bernevig, Magnetic topological quantum chemistry, *Nature Communications* **12**, 5965 (2021).
 - [42] L. Sheng, A. Duvakina, H. Wang, K. Yamamoto, R. Yuan, J. Wang, P. Chen, W. He, K. Yu, Y. Zhang, J. Chen, J. Hu, W. Song, S. Liu, X. Han, D. Yu, J. Ansermet, S. Maekawa, D. Grundler, and H. Yu, Control of spin currents by magnon interference in a canted antiferromagnet, *Nat. Phys.* **21**, 740 (2025).
 - [43] H. Wang, R. Yuan, Y. Zhou, Y. Zhang, J. Chen, S. Liu, H. Jia, D. Yu, J. Ansermet, C. Song, and H. Yu, Long-

- distance coherent propagation of high-velocity antiferromagnetic spin waves, *Phys. Rev. Lett.* **130**, 096701 (2023).
- [44] A. El Kanj, O. Gomonay, I. Boventer, P. Bortolotti, V. Cros, A. Anane, and R. Lebrun, Antiferromagnetic magnon spintronic based on nonreciprocal and nondegenerated ultra-fast spin-waves in the canted antiferromagnet α -Fe₂O₃, *Sci. Adv.* **9**, eadh1601 (2023).
- [45] J. Chen, Z. Jin, R. Yuan, H. Wang, H. Jia, W. Wei, L. Sheng, J. Wang, Y. Zhang, S. Liu, *et al.*, Observation of coherent gapless magnons in an antiferromagnet, *Phys. Rev. Lett.* **134**, 056701 (2025).
- [46] F. Moussa, M. Hennion, J. Rodriguez-Carvajal, H. Moudden, L. Pinsard, and A. Revcolevschi, Spin waves in the antiferromagnet perovskite LaMnO₃: A neutron-scattering study, *Phys. Rev. B* **54**, 15149 (1996).
- [47] T. Weber, J. Waizner, P. Steffens, A. Bauer, C. Pfleiderer, M. Garst, and P. Böni, Polarized inelastic neutron scattering of nonreciprocal spin waves in MnSi, *Phys. Rev. B* **100**, 060404 (2019).
- [48] Y. Nambu, J. Barker, Y. Okino, T. Kikkawa, Y. Shiomi, M. Enderle, T. Weber, B. Winn, M. Graves-Brook, J. M. Tranquada, *et al.*, Observation of magnon polarization, *Phys. Rev. Lett.* **125**, 027201 (2020).
- [49] M. V. Berry, The quantum phase, five years after, in *Geometric phases in physics*, Adv. Ser. Math. Phys., Vol. 5, edited by A. Shapere and F. Wilczek (World Scientific, Singapore, 1989) pp. 7–28.
- [50] J. Provost and G. Vallée, Riemannian structure on manifolds of quantum states, *Commun. Math. Phys.* **76**, 289 (1980).
- [51] Q. Niu, D. J. Thouless, and Y. Wu, Quantized Hall conductance as a topological invariant, *Phys. Rev. B* **31**, 3372 (1985).
- [52] C. L. Kane and E. J. Mele, Z₂ topological order and the quantum spin Hall effect, *Phys. Rev. Lett.* **95**, 146802 (2005).
- [53] N. Nagaosa, J. Sinova, S. Onoda, A. H. MacDonald, and N. P. Ong, Anomalous Hall effect, *Rev. Mod. Phys.* **82**, 1539 (2010).
- [54] J. Sinova, S. O. Valenzuela, J. Wunderlich, C. H. Back, and T. Jungwirth, Spin Hall effects, *Rev. Mod. Phys.* **87**, 1213 (2015).
- [55] A. Bouhon, A. Timmel, and R.-J. Slager, Quantum geometry beyond projective single bands, *arXiv preprint arXiv:2303.02180* (2023).
- [56] N. Wang, D. Kaplan, Z. Zhang, T. Holder, N. Cao, A. Wang, X. Zhou, F. Zhou, Z. Jiang, C. Zhang, N. Wang, *et al.*, Quantum-metric-induced nonlinear transport in a topological antiferromagnet, *Nature* **621**, 487 (2023).
- [57] A. Gao, Y.-F. Liu, J.-X. Qiu, B. Ghosh, T. V. Trevisan, Y. Onishi, C. Hu, T. Qian, H. Tien, S.-W. Chen, *et al.*, Quantum metric nonlinear Hall effect in a topological antiferromagnetic heterostructure, *Science* **381**, 181 (2023).
- [58] M. Schüler, U. De Giovannini, H. Hübener, A. Rubio, M. A. Sentef, and P. Werner, Local Berry curvature signatures in dichroic angle-resolved photoelectron spectroscopy from two-dimensional materials, *Sci. Adv.* **6**, eaay2730 (2020).
- [59] G. E. Topp, C. J. Eckhardt, D. M. Kennes, M. A. Sentef, and P. Törmä, Light-matter coupling and quantum geometry in moiré materials, *Phys. Rev. B* **104**, 064306 (2021).
- [60] J. Ahn, G. Guo, N. Nagaosa, and A. Vishwanath, Riemannian geometry of resonant optical responses, *Nat. Phys.* **18**, 290 (2022).
- [61] E. Viñas Boström, T. S. Parvini, J. W. McIver, A. Rubio, S. V. Kusminskiy, and M. A. Sentef, Direct optical probe of magnon topology in two-dimensional quantum magnets, *Phys. Rev. Lett.* **130**, 026701 (2023).
- [62] S. Kim, Y. Chung, Y. Qian, S. Park, C. Jozwiak, E. Rotenberg, A. Bostwick, K. S. Kim, and B.-J. Yang, Direct measurement of the quantum metric tensor in solids, *Science* **388**, 1050 (2025).
- [63] M.-H. Zhang, G. Xuan, and D.-X. Yao, Dirac points and Weyl phase in a honeycomb altermagnet, *arXiv preprint arXiv:2412.03657* (2024).
- [64] W. Lu, S. Feng, Y. Wang, D. Chen, Z. Lin, X. Liang, S. Liu, W. Feng, K. Yamagami, J. Liu, *et al.*, Signature of topological surface bands in altermagnetic Weyl semimetal CrSb, *Nano Lett.* **25**, 7343 (2025).
- [65] Y. Fang, J. Cano, and S. A. A. Ghorashi, Quantum geometry induced nonlinear transport in altermagnets, *Phys. Rev. Lett.* **133**, 106701 (2024).
- [66] L. Han, X. Fu, C. Song, Y. Zhu, X. Li, Z. Zhu, H. Bai, R. Chu, J. Dai, S. Liang, *et al.*, Discovery of a large magnetic nonlinear Hall effect in an altermagnet, *arXiv preprint arXiv:2502.04920* (2025).
- [67] W. Chen, X. Zhou, W.-K. Lou, and K. Chang, Magneto-optical conductivity and circular dichroism in d-wave altermagnets, *Phys. Rev. B* **111**, 064428 (2025).
- [68] T. Nag, R.-J. Slager, T. Higuchi, and T. Oka, Dynamical synchronization transition in interacting electron systems, *Phys. Rev. B* **100**, 134301 (2019).
- [69] T. V. Trevisan, P. V. Arribi, O. Heinonen, R.-J. Slager, and P. P. Orth, Bicircular light Floquet engineering of magnetic symmetry and topology and its application to the Dirac semimetal Cd₃As₂, *Phys. Rev. Lett.* **128**, 066602 (2022).
- [70] Y. Ikeda, S. Kitamura, and T. Morimoto, Photocurrent induced by a bicircular light drive in centrosymmetric systems, *Phys. Rev. Lett.* **131**, 096301 (2023).
- [71] K. Shen, Magnon spin relaxation and spin Hall effect due to the dipolar interaction in antiferromagnetic insulators, *Phys. Rev. Lett.* **124**, 077201 (2020).
- [72] J. Liu, L. Wang, and K. Shen, Dipolar spin waves in uniaxial easy-axis antiferromagnets: A natural topological nodal-line semimetal, *Phys. Rev. Res.* **2**, 023282 (2020).
- [73] J. Liu, L. Wang, and K. Shen, Tunable topological magnon phases in layered ferrimagnets, *Phys. Rev. B* **107**, 174404 (2023).
- [74] B. Bermond, A. Defossez, N. Goldman, *et al.*, A local quantized marker for topological magnons from circular dichroism, *arXiv preprint arXiv:2504.17374* (2025).
- [75] E. Syljuåsen, A. Qaiumzadeh, and A. Sudbø, Quantum geometry and magnon Hall transport in an altermagnet, *arXiv preprint arXiv:2505.04726* (2025).
- [76] Z. Jin, H. Yang, Z. Zeng, Y. Cao, and P. Yan, Cavity-induced strong magnon-magnon coupling in altermagnets, *arXiv preprint arXiv:2307.00909* (2023).
- [77] T. Holstein and H. Primakoff, Field dependence of the intrinsic domain magnetization of a ferromagnet, *Phys. Rev.* **58**, 1098 (1940).
- [78] J. Colpa, Diagonalization of the quadratic boson Hamiltonian, *Physica A* **93**, 327 (1978).
- [79] I. Araya Day, A. Varentcova, D. Varjas, and A. R. Akhmerov, Pfaffian invariant identifies magnetic ob-

- structed atomic insulators, *SciPost Phys.* **15**, 114 (2023).
- [80] Y. Onose, T. Ideue, H. Katsura, Y. Shiomi, N. Nagaosa, and Y. Tokura, Observation of the magnon Hall effect, *Science* **329**, 297 (2010).
- [81] M. dos Santos Dias, N. Biniskos, F. J. dos Santos, L. Perini, L. S. Cavalcante, D. Sander, S. Lounis, *et al.*, Topological magnons driven by the Dzyaloshinskii-Moriya interaction in the centrosymmetric ferromagnet Mn_5Ge_3 , *Nat. Commun.* **14**, 7321 (2023).
- [82] See Supplemental Material (SM) at [url] for details on the light-magnon coupling up to the fourth order (Sec. I), comparison of altermagnetic and antiferromagnetic models (Sec. II), and further analytical details on the bicircular Raman response (Sec. III).
- [83] Y. R. Shen and N. Bloembergen, Interaction between light waves and spin waves, *Phys. Rev.* **143**, 372 (1966).
- [84] W. J. Jankowski, A. S. Morris, A. Bouhon, F. N. Ünal, and R.-J. Slager, Optical manifestations and bounds of topological Euler class, *Phys. Rev. B* **111**, L081103

(2025).

- [85] G. Chaudhary, M. Levin, and A. A. Clerk, Simple approach to characterizing band topology in bosonic pairing Hamiltonians, *Phys. Rev. B* **103**, 214306 (2021).
- [86] I. Tesfaye, A. Eckardt, *et al.*, Quantum geometry of bosonic Bogoliubov quasiparticles, *arXiv preprint arXiv:2406.12981* (2024).

END MATTER

Appendix A: Details of the effective altermagnetic Hamiltonians.— Below, we provide further technical details on the d -wave altermagnet model studied in this work [76]. In real space, the spin Heisenberg Hamiltonian \mathcal{H} written in terms of the lattice spin operators $\mathbf{S}_i^\uparrow, \mathbf{S}_i^\downarrow$, which we consider in this work, reads,

$$\begin{aligned} \mathcal{H} = & - \left(\sum_{\langle ij \rangle_x} J_1 \mathbf{S}_i^\uparrow \cdot \mathbf{S}_j^\uparrow + \sum_{\langle ij \rangle_y} J_2 \mathbf{S}_i^\uparrow \cdot \mathbf{S}_j^\uparrow \right) - \left(\sum_{\langle ij \rangle_x} J_2 \mathbf{S}_i^\downarrow \cdot \mathbf{S}_j^\downarrow + \sum_{\langle ij \rangle_y} J_1 \mathbf{S}_i^\downarrow \cdot \mathbf{S}_j^\downarrow \right) - \sum_i J_{\text{AFM}} \mathbf{S}_i^\uparrow \cdot \mathbf{S}_i^\downarrow \\ & - \frac{1}{2} K \sum_i \left[(\mathbf{S}_i^\uparrow \cdot \hat{\mathbf{z}})^2 + (\mathbf{S}_i^\downarrow \cdot \hat{\mathbf{z}})^2 \right] - g\mu_B H_0 \sum_i (\mathbf{S}_i^\uparrow + \mathbf{S}_i^\downarrow) \cdot \hat{\mathbf{x}}, \end{aligned} \quad (2)$$

with $J_{1,2} = J \pm \Delta J$ the intrasublattice exchange coupling coefficient, $J_{\text{AFM}} < 0$ the intersublattice antiferromagnetic exchange coupling coefficient, $K > 0$ the easy-axis magnetic anisotropy, $\hat{\mathbf{x}}, \hat{\mathbf{z}}$ the unit vectors in the x and z directions, the Bohr magneton μ_B , Landé g -factor, and H_0 an external field along x direction, which cants the sublattices, see Fig. 1(a). ΔJ gives the scale of altermagnetic splitting of magnons, and $\langle ij \rangle_{x,y}$ denotes the nearest neighbors in the x, y directions, respectively.

Under the Holstein-Primakoff transformation employed to capture the chirality of magnons in the main text, the corresponding momentum-space magnon Hamiltonian amounts to,

$$\begin{aligned} \mathcal{H}^{\mathbf{k}} = & (A_1 - A_2) \sigma_0 \tau_0 + (A_1 + A_2) \sigma_3 \tau_0 \\ & + B_1 \sigma_1 \tau_1 + B_2 \sigma_1 \tau_0. \end{aligned} \quad (3)$$

In the above, the model parameters read:

$$\begin{aligned} A_{1,2} = & \hbar S [J_{1,2} (1 - \cos k_x) + J_{2,1} (1 - \cos k_y) \\ & + K/2 - \cos 2\theta J_{\text{AFM}}/2 + g\mu_B H_0 \sin \theta/2], \\ B_1 = & \hbar S J_{\text{AFM}} (1 + \cos 2\theta)/2, \\ B_2 = & -\hbar S J_{\text{AFM}} (1 - \cos 2\theta)/2, \end{aligned} \quad (4)$$

where $\theta = \arctan[g\mu_B S H_0 / (2J_{\text{AFM}})]$ is the canting angle induced by the external magnetic field H_0 , and $\sigma_{0,1,2,3}$ ($\tau_{0,1,2,3}$) denote the Pauli matrices operating on sublattice (wavevector) degree of freedom, respectively.

Appendix B: Details of quantum geometry of altermagnetic magnons.— In the following, we provide further technical details on the unique quantum geometry of altermagnetic magnons retrieved and probed by light in this work. The magnonic metric $g_{ab}^{(\text{m})}$ considered in the main text, reads in terms of magnonic band eigenvectors $|u_i\rangle \equiv [U]_i$,

$$g_{ab}^{(\text{m})} = \text{Re} \frac{([\bar{U}]_1 \tau_3 \partial_{k_a} \mathcal{H}^{\mathbf{k}}[U]_2) ([\bar{U}]_2 \tau_3 \partial_{k_b} \mathcal{H}^{\mathbf{k}}[U]_1)}{(\omega_1 - \omega_2)^2}, \quad (5)$$

consistently with Ref. [61], where we set $\hbar = 1$. We emphasize that the quantum geometry of magnons driven by the considered BdG Hamiltonians is fundamentally a symplectic quantum geometry [61, 85, 86]. We now detail how the nontrivial metric texture [Fig. 3(a)], which reflects the chirality (p_j) alteration, and its coincidence with the $L_{ab}^{(2)}$ pattern [Fig. 3(b)] identified in the main text, arise. The enhancement of diagonal terms $g_{aa}^{(\text{m})}$ [Fig. 3(a)] definitionally occurs under a local \mathbf{k} -space condition: $|([\bar{U}]_1 \tau_3 \partial_{k_a} \mathcal{H}^{\mathbf{k}}[U]_2)|^2 \gg 1$. These matrix elements, equivalently translate to a local enhancement of matrix elements $|\bar{U}^\dagger U_a|$ occurring in the LMC matrix elements, i.e., $L_a^{(1)}$ and $L_{ab}^{(2)}$, as defined in the main text, and consistently with the identifications of Ref. [61]. Furthermore, within an analogous argument, we retrieve additional geometric enhancements in the fourth-order light-magnon coupling $L_{abcd}^{(4)}$, which we explicitly demonstrate

in the SM [82].

Crucially, the matrix elements $|\bar{U}^\dagger U_a|$ closely reflect the magnon chirality features. On direct differentiation, the gradient $\nabla_{\mathbf{k}} p_j$, introduced by the unique alteration of altermagnetic magnonic chirality (p_j), definitionally consists of the terms $(U_{ij}^{-1})^* \nabla_{\mathbf{k}} U_{ij}^{-1}$. The gradients of U_{ij}^{-1}

inverses in the individual magnon bands i , within the $(U_{ij}^{-1})^* \nabla_{\mathbf{k}} U_{ij}^{-1}$ terms, translate into the enhancements in the matrix elements $|\bar{U}^\dagger U_a|$. As we explain above, these are central to the LMC and magnonic quantum metric $g_{ab}^{(m)}$. To visualize these relations quantitatively, we present the \mathbf{k} -space resolved local patterns in Fig. 2(a)–Fig. 2(b) against the textures in Fig. 3(a)–Fig. 3(b).

SUPPLEMENTAL MATERIAL

Quantum Geometry of Altermagnetic Magnons Probed by Light

Rundong Yuan,^{1,*} Wojciech J. Jankowski,^{1,†} Ka Shen,^{2,3} and Robert-Jan Slager^{4,1,‡}

¹*TCM Group, Cavendish Laboratory, University of Cambridge, J. J. Thomson Avenue, Cambridge CB3 0HE, United Kingdom*

²*The Center for Advanced Quantum Studies and School of Physics and Astronomy,
Beijing Normal University, Beijing 100875, China*

³*Key Laboratory of Multiscale Spin Physics, Ministry of Education,
Beijing Normal University, Beijing 100875, China*

⁴*Department of Physics and Astronomy, University of Manchester, Oxford Road, Manchester M13 9PL, United Kingdom*
(Dated: August 6, 2025)

CONTENTS

I. Light-magnon coupling up to the fourth order	2
II. Comparison of altermagnetic and antiferromagnetic models	3
III. Further analytical details on the bicircular Raman response	4
References	4

* ry306@cam.ac.uk

† wjj25@cam.ac.uk

‡ rjs269@cam.ac.uk

I. LIGHT-MAGNON COUPLING UP TO THE FOURTH ORDER

The general light-magnon coupling [1] up to the fourth order in the electromagnetic fields reads,

$$\mathcal{H}^{\mathbf{k}}(\mathbf{A}) = \mathcal{H}^{\mathbf{k}} + L_a^{(1)} A_a + L_{ab}^{(2)} A_a A_b + L_{abc}^{(3)} A_a A_b A_c + L_{abcd}^{(4)} A_a A_b A_c A_d, \quad (1)$$

where $\mathbf{A} = (A_x, A_y, A_z)$ is the electromagnetic vector potential. $\mathbf{L}^{(n)}$ are the light-matter coupling (LMC) matrix elements [2, 3]. Upon applying the normalization condition to Bogoliubov transformation we obtain an effective Schrödinger equation $\mathcal{H}^{\mathbf{k}} U = \bar{U} \Omega^{\mathbf{k}}$. On differentiating both sides and multiplying by U^\dagger on the left, we obtain:

$$U^\dagger \mathcal{H}_a^{\mathbf{k}} U = \Omega_a + U^\dagger \bar{U}_a \Omega - \Omega \bar{U}^\dagger U_a, \quad (2)$$

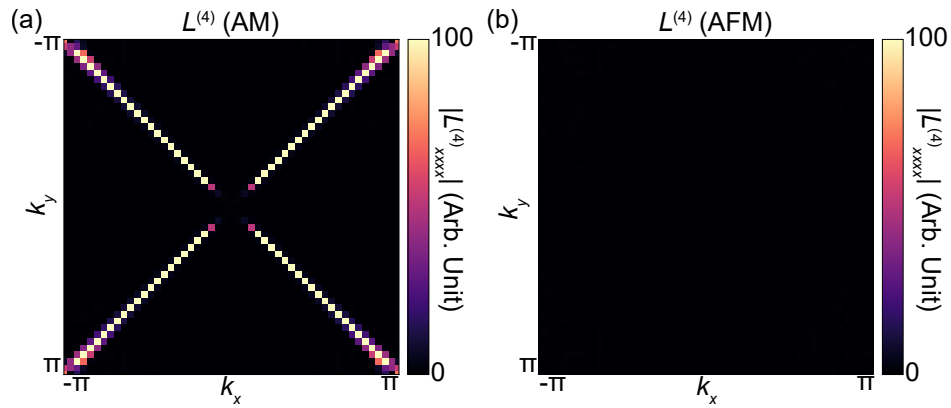
where we use a matrix with subscript a to represent that the matrix is differentiated by $\partial/\partial k_a$, and a runs over all directions x, y, z . Eq. (2) gives the first-order LMC coefficient as $L_a^{(1)} = -U^\dagger \mathcal{H}_a^{\mathbf{k}} U$. Similarly, we can differentiate the effective Schrödinger equation two, three, and four times to deduce $L_{ab}^{(2)}$, $L_{abc}^{(3)}$, and $L_{abcd}^{(4)}$. Consistently, the subscripts b, c, d also run over all x, y, z . The LMC coefficients up to the fourth order are compactly retrieved as follows:

$$L_{ab}^{(2)} = L_a^{(1)} \bar{U}^\dagger U_b - \frac{1}{2} \Omega \bar{U}^\dagger U_{ab} + \frac{1}{2} U^\dagger \bar{U}_{ab} \Omega + U^\dagger \bar{U}_a \Omega_b + \frac{1}{2} \Omega_{ab} + (ab \rightarrow \{ab\}), \quad (3)$$

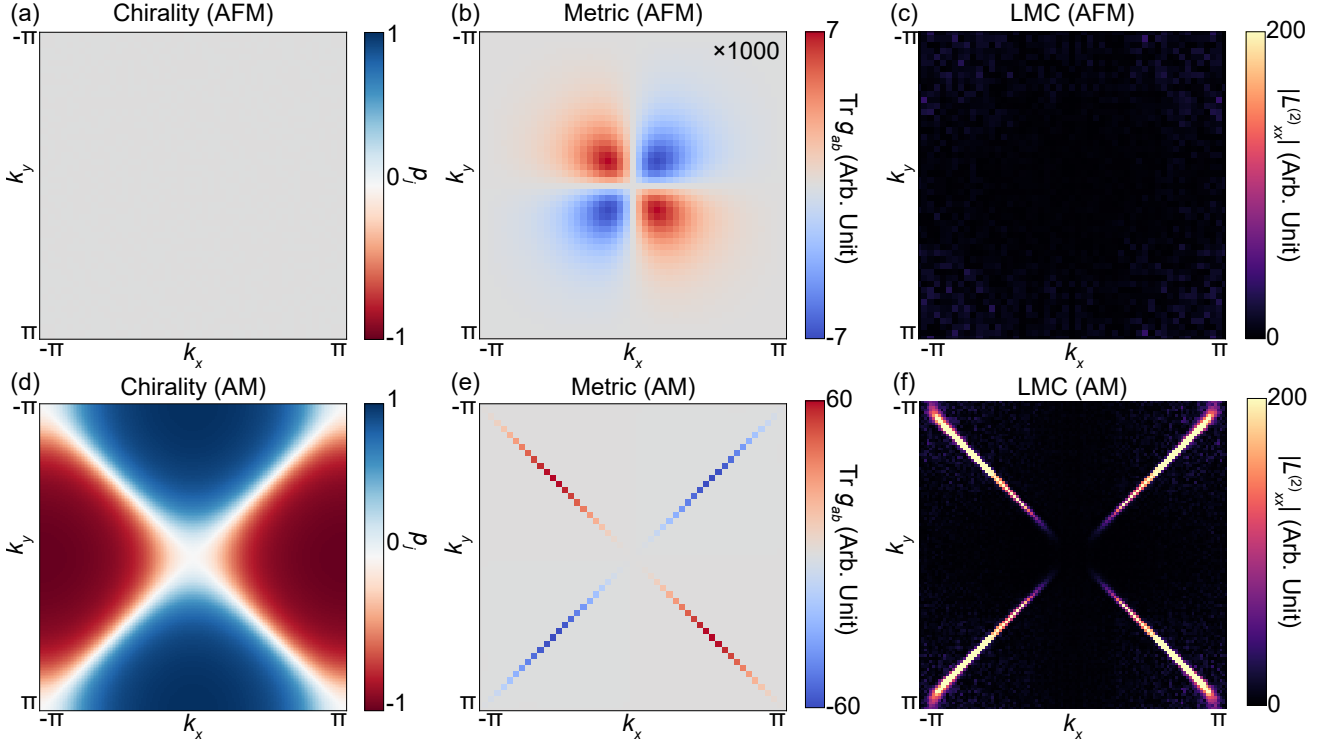
$$L_{abc}^{(3)} = -\frac{1}{6} U^\dagger \bar{U}_{abc} \Omega - \frac{1}{2} U^\dagger \bar{U}_{ab} \Omega_c - \frac{1}{2} U^\dagger \bar{U}_a \Omega_{bc} - \frac{1}{6} \Omega_{abc} + \frac{1}{2} L_{ab}^{(2)} \bar{U}^\dagger U_c - \frac{1}{2} L_a^{(1)} \bar{U}^\dagger U_{bc} + \frac{1}{6} \Omega \bar{U}^\dagger U_{abc} + (abc \rightarrow \{abc\}), \quad (4)$$

$$L_{abcd}^{(4)} = \frac{1}{6} L_{abc}^{(3)} \bar{U}^\dagger U_d - \frac{1}{4} L_{ab}^{(2)} \bar{U}^\dagger U_{cd} + \frac{1}{6} L_a^{(1)} \bar{U}^\dagger U_{bcd} - \frac{1}{24} \Omega \bar{U}^\dagger U_{abcd} + \frac{1}{24} U^\dagger \bar{U}_{abcd} \Omega + \frac{1}{6} U^\dagger \bar{U}_{abc} \Omega_d + \frac{1}{4} U^\dagger \bar{U}_{ab} \Omega_{cd} + \frac{1}{6} U^\dagger \bar{U}_a \Omega_{bcd} + \frac{1}{24} \Omega_{abcd} + (abcd \rightarrow \{abcd\}), \quad (5)$$

where $+(abcd \rightarrow \{abcd\})$, etc., indicate that the equation is summing over all permutations. Below, we show the momentum-space profile of $L_{abcd}^{(4)}$ in the d -wave altermagnet model studied in the main text, against $L_{abcd}^{(4)}$ realized in an antiferromagnetic phase of the model ($\Delta J = 0$). For further comparison of the altermagnetic and antiferromagnetic phases, see also the next Section.



SUPPLEMENTAL FIG. 1. Fourth-order light-magnon coupling matrix elements, $L_{abcd}^{(4)}$, in (a) an altermagnetic (AM) model studied in the main text, and (b) the corresponding antiferromagnetic (AFM) model. Although, the associated fourth-order responses are negligible compared to the second-order nonlinear coupling $L_{ab}^{(2)}$ central to the main text, the AFM notably realizes orders-of-magnitude smaller fourth-order nonlinearity, as compared to the AM phase.

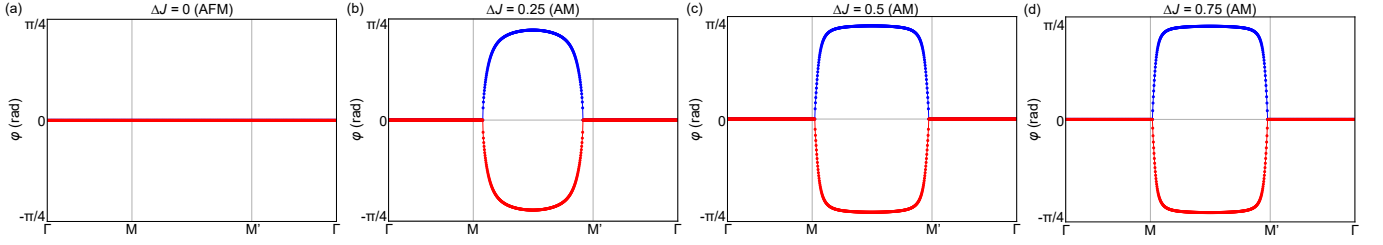


SUPPLEMENTAL FIG. 2. Comparison of the lowest magnon band chiralities (a,d), magnonic quantum metrics (b,e), and light-magnon couplings (c,f) in an antiferromagnetic (AFM) model (a)–(c), against the altermagnetic (AM) model (d)–(f) studied in the main text.

II. COMPARISON OF ALTERMAGNETIC AND ANTIFERROMAGNETIC MODELS

In this section we compare our main findings in altermagnets against the conventional antiferromagnets. The parameterization of our model is the same as in the main text, with a different altermagnetic splitting: $\Delta J = 0$. We also consistently apply a magnetic field along the x direction. In Fig. S2(a), we show the chirality of magnons in antiferromagnets with the same color bar as for the altermagnet in the main text. In the considered model, we find that the magnons with left- and right- handed chirality are degenerate over the full Brillouin zone (BZ) in the antiferromagnetic state. The degeneracy is expected, since the magnetic field is perpendicular to the Néel vector. Hence, there is no altering chirality in the antiferromagnetic model, unlike in the corresponding altermagnetic case. We then calculate the magnonic quantum metric of the system, and find that the metric, and its trace, are much smaller than in the altermagnetic setting, as shown in Fig. S2(b). We note that in the main text we retrieve a vast range of values (± 60), as captured by the color bar, while in Fig. S2(b), a significantly smaller range of ± 0.007 is found within an antiferromagnetic phase. The quantum metric result is compatible with the claim of our main text that without altering the chirality across BZ, there is no nontrivial metric texture in the system. We also calculate the \mathbf{k} -resolved nonlinear LMC terms which is shown in Fig. S2(c). As represented using the same color bar as in the main text, we find three orders of magnitude smaller response encoded in the LMC within the antiferromagnetic model, which also verifies our main claim. Furthermore, for a direct comparison, we include the analogous results for the altermagnet studied in the main text [Fig. S2(d)–Fig. S2(f)], to manifestly show these major distinctions between the antiferromagnetic and altermagnetic magnon states.

Finally, in Fig. S3, we directly demonstrate how the geometric phases captured by the magnonic Wilson loop compare between the antiferromagnetic ($\Delta J = 0$) [Fig. S3(a)] and altermagnetic ($\Delta J \neq 0$) [Fig. S3(b)–Fig. S3(d)] model realizations. We confirm that, unlike in the altermagnetic magnon bands, the antiferromagnets realize no nontrivial features in magnonic geometry. Namely, we find that the magnonic Wilson loop eigenvalues are trivial ($\phi = 0$) in the antiferromagnet, consistently with the chirality arguments provided in the main text.



SUPPLEMENTAL FIG. 3. Comparison of the magnonic Wilson loops in (a) antiferromagnetic (AFM) phase ($\Delta J = 0$), against the (b)–(d) altermagnetic (AM) magnons ($\Delta J \neq 0$).

III. FURTHER ANALYTICAL DETAILS ON THE BICIRCULAR RAMAN RESPONSE

In the following, we provide further analytical details on the bicircular Raman response underpinned by the outlined LMC perturbations, as retrieved numerically in the main text. We further elucidate the phase delay (α) dependence of the optical response. On inserting the bicircular light form introduced in the main text to the general LMC Hamiltonian, Eq. (1), we have,

$$\mathcal{H}^{\mathbf{k}}(\mathbf{A}) = \mathcal{H}^{\mathbf{k}} + L_a^{(1)}(\mathbf{A}_L e^{i(\omega_{\text{in}} t + \alpha)} + \mathbf{A}_R e^{-i\omega_{\text{in}} t})_a + L_{ab}^{(2)}(\mathbf{A}_L e^{i(\omega_{\text{in}} t + \alpha)} + \mathbf{A}_R e^{-i\omega_{\text{in}} t})_a (\mathbf{A}_L e^{i(\omega_{\text{in}} t + \alpha)} + \mathbf{A}_R e^{-i\omega_{\text{in}} t})_b. \quad (6)$$

Here we truncated the LMC at the second order in optical fields, as justified in the previous sections. On setting equal strengths (A_0) for left- and right- circularly-polarized components $\mathbf{A}_{L/R} = A_0 \hat{\mathbf{e}}_{\pm} \equiv A_0 \frac{\hat{\mathbf{x}} \pm i\hat{\mathbf{y}}}{\sqrt{2}}$, with $\hat{\mathbf{x}}, \hat{\mathbf{y}}$ the unit polarization vectors along x and y directions, we further simplify the considered bicircular coupling to,

$$\begin{aligned} \mathcal{H}^{\mathbf{k}}(\mathbf{A}) = \mathcal{H}^{\mathbf{k}} + \frac{|A_0|}{\sqrt{2}} L_a^{(1)} [(\hat{\mathbf{x}} + i\hat{\mathbf{y}}) e^{i(\omega_{\text{in}} t + \alpha)} + (\hat{\mathbf{x}} - i\hat{\mathbf{y}}) e^{-i\omega_{\text{in}} t}]_a \\ + \frac{|A_0|^2}{2} L_{ab}^{(2)} [(\hat{\mathbf{x}} + i\hat{\mathbf{y}}) e^{i(\omega_{\text{in}} t + \alpha)} + (\hat{\mathbf{x}} - i\hat{\mathbf{y}}) e^{-i\omega_{\text{in}} t}]_a [(\hat{\mathbf{x}} + i\hat{\mathbf{y}}) e^{i(\omega_{\text{in}} t + \alpha)} + (\hat{\mathbf{x}} - i\hat{\mathbf{y}}) e^{-i\omega_{\text{in}} t}]_b, \end{aligned} \quad (7)$$

$$\begin{aligned} \mathcal{H}^{\mathbf{k}}(\mathbf{A}) = \mathcal{H}^{\mathbf{k}} + \sqrt{2} |A_0| e^{i\alpha/2} L_a^{(1)} [\hat{\mathbf{x}} \cos(\omega_{\text{in}} t + \alpha/2) - \hat{\mathbf{y}} \sin(\omega_{\text{in}} t + \alpha/2)]_a \\ + 2 |A_0|^2 e^{i\alpha} L_{ab}^{(2)} [\hat{\mathbf{x}} \cos(\omega_{\text{in}} t + \alpha/2) - \hat{\mathbf{y}} \sin(\omega_{\text{in}} t + \alpha/2)]_a [\hat{\mathbf{x}} \cos(\omega_{\text{in}} t + \alpha/2) - \hat{\mathbf{y}} \sin(\omega_{\text{in}} t + \alpha/2)]_b. \end{aligned} \quad (8)$$

The choice of individual indices $a, b = x, y$ in LMC selects distinct α -dependent components: $\hat{\mathbf{x}} \cos(\omega_{\text{in}} t + \alpha/2)$ and $\hat{\mathbf{y}} \sin(\omega_{\text{in}} t + \alpha/2)$. For $L_{xx}^{(2)}$ component shown in the main text, the strictly nonnegative term: $|A_0|^2 \cos^2(\omega_{\text{in}} t + \alpha/2)$ competes with: $|A_0| \cos(\omega_{\text{in}} t + \alpha/2)$, for the $L_x^{(1)}$ coupling. Notably, the $L_x^{(1)}$ and $L_{xx}^{(2)}$ terms have different phase-dependences in the corresponding amplitudes related to the power absorption, independently from the time-averaging of the oscillatory terms. Averaging the cross-sections over the range of bicircular phase delay parameter α allows to distinguish the magnitudes of $L_x^{(1)}$ and $L_{xx}^{(2)}$ related to the magnonic metric $g_{ab}^{(m)}$, as pointed out in the main text. More precisely, inserting the LMC in the Fermi's golden rule expression [2] for Raman scattering, the matrix elements of the above bicircular LMC, combined with their conjugates, introduce distinct phase-shift dependences on α for $L_a^{(1)}$ and $L_{ab}^{(2)}$ contributions. Hence, the dependences of the bicircular Raman scattering cross-section on α allows to specifically target $L_{ab}^{(2)}$, which reflects the magnonic quantum metric tensor $g_{ab}^{(m)}$ [2], as described in the main text.

-
- [1] Y. R. Shen and N. Bloembergen, Interaction between light waves and spin waves, Phys. Rev. **143**, 372 (1966).
 - [2] G. E. Topp, C. J. Eckhardt, D. M. Kennes, M. A. Sentef, and P. Törmä, Light-matter coupling and quantum geometry in moiré materials, Phys. Rev. B **104**, 064306 (2021).
 - [3] E. Viñas Boström, T. S. Parvini, J. W. McIver, A. Rubio, S. V. Kusminskiy, and M. A. Sentef, Direct optical probe of magnon topology in two-dimensional quantum magnets, Phys. Rev. Lett. **130**, 026701 (2023).